Wave2Web: Near-real-time reservoir availability prediction for water security in India

Lucas Kruitwagen[a,b,*], Chris Arderne[a,b], Thomas Lees[a], Lisa Thalheimer[a], Samantha Kuzma[c], Samrat Basak[d]

a: H2Ox, School of Geography and the Environment, University of Oxford, South Parks Road, Oxford, OX1 3QY, United Kingdom
b: Oxford Earth Observation Ltd., Oxford, United United Kingdom
c: World Resources Institute, 10 G Street, NE Suite 800, Washington DC, 20002, United States
d: World Resources Institute India, 2nd Floor, No. 93/2, G Towers, South End Road, Basavanagudi, Bengaluru, 560004, India
* Corresponding Author: lucas.kruitwagen@gmail.com

Graphical Abstract

Wave2Web: Near-real-time reservoir availability prediction for water security in India

Lucas Kruitwagen, Chris Arderne, Thomas Lees, Lisa Thalheimer, Samantha Kuzma, Samrat Basak

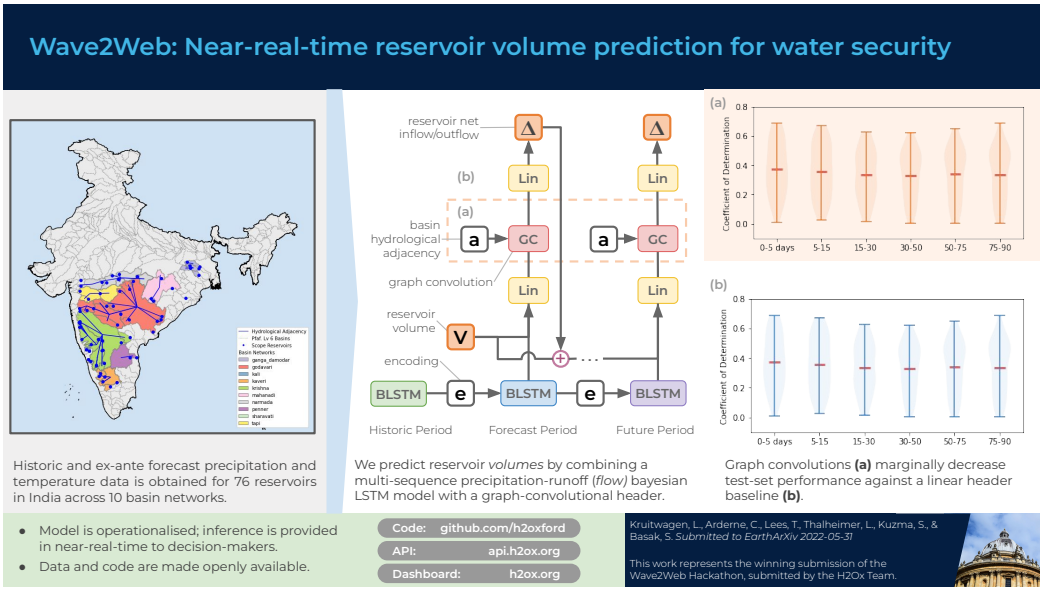

Highlights

Wave2Web: Near-real-time reservoir availability prediction for water security in India

Lucas Kruitwagen, Chris Arderne, Thomas Lees, Lisa Thalheimer, Samantha Kuzma, Samrat Basak

- We build an autocorrelative sequence-to-sequence-to-sequence bayesian LSTM with a graph convolutional header to predict daily water availability changes in reservoir networks.
- We train multiple models to predict ninety-day volumetric water availability changes across sixty-six reservoirs in ten reservoir networks in India.
- We deploy our models and build a dataservice that ingests meteorological data and current reservoir levels, offering predictions in near-real-time for decision-makers and stakeholders.

Wave2Web: Near-real-time reservoir availability prediction for water security in India

Lucas Kruitwagen[a,b], Chris Arderne[a,b], Thomas Lees[a], Lisa Thalheimer[a], Samantha Kuzma[c], Samrat Basak[d]

[a] *H2Ox, School of Geography and the Environment, University of Oxford, South Parks Road, Oxford, OX1 3QY, United Kingdom*
[b] *Oxford Earth Observation Ltd., Oxford, United United Kingdom*
[c] *World Resources Institute, 10 G Street, NE Suite 800, Washington DC, 20002, United States*
[d] *World Resources Institute India, 2nd Floor, No. 93/2, G Towers, South End Road, Basavanagudi, Bengaluru, 560004, India*

Abstract

By 2050, over half the world's population will live in water-stressed areas.[1] Medium-term drought forecasting can help planners avoid "day-zero" events and adapt to climate change. Machine learning-based precipitation-runoff modelling enables the prediction of surface water flow using only the meteorological record of a water basin. In this work, we extend a Bayesian LSTM precipitation-runoff model with graph convolutions based on hydrological basin adjacency to predict reservoir water availability for sixty-six reservoirs in India. Employing a "sequence-to-sequence-to-sequence" model allows predictions to be based on the combination of meteorological forcing data and ex-ante forecast data while producing predictions to a ninety-day future horizon. On a held-back test set of daily reservoir water availability changes, we achieve a coefficient of determination of 0.372 for the maximum likelihood estimate for the 1-to-5 day horizon averaged across all sites, which reduces to 0.337 for the 75-to-90 day horizon. We also find that removing the graph convolutional layer *increases* mean performance by 0.82 percentage points over the same horizons. This work represents the winning submission of the Wave2Web hackathon; the code and data is publicly available and near-real-time predictions are available at h2ox.org.

Email address: lucas.kruitwagen@gmail.com (Lucas Kruitwagen)

Keywords: hydrology, deep learning, LSTM, graph convolution

1. Introduction

More frequent and severe drought is one of the most rapidly emerging impacts of climate change. Planners and water system operators can adapt to changing drought conditions by better anticipating water shortages and taking preventative measures including the construction of new infrastructure, efficiency and conservation upgrades, and curtailment. Hydrological drought, the condition describing decreased water availability for end-users, combines the conditions of meteorological drought (i.e. below-average rainfall) with decreased or constrained surface- and groundwater availability [2]. To address acute hydrological stress, planners need visibility not only of the forecast rainfall, but also current and projected hydrological conditions in their catchments of interest. Operational forecasts are required to enable more effective water management decisions, and the information produced must be provided in near-real-time, allowing operators to take anticipatory action in response to changing conditions.

India is one of the most water-stressed countries in the world. In 2020, the basins in India with "high" or "extremely high" water stress[3] were home to 690mn people,[4] 59mn ha of agricultural land,[5] and 32% of India's thermal electricity generation capacity[6]. 25% of India's households do not have access to on-premesis drinking water, and India extracts more groundwater than any other country[7]. Some parts of Chennai, a city of 11mn in Tamil Nadu, experienced a 'day zero' water scarcity event in 2019; Bengaluru (population of 13mn, Karnataka) has only narrowly avoided a similar catastrophe. There is an urgent need for anticipatory water management in India's primary reservoir networks to assist in responsible water use prioritization and better water allocation to various water users. In this study, we prepare and deploy a machine learning model to predict surface water availability in sixty-six reservoirs across ten basin networks. The basin networks, reservoirs, and their hydrological adjacency is shown in Figure 1.

Deep neural networks are the currently best-available models for prediction tasks in hydrological systems [8, 9, 10, 11, 12]. Recurrent neural networks in particular, which take advantage of the sequential nature of the timeseries data, have been used to forecast river flow (e.g. Nagesh Kumar et al. [9], Kratzert et al. [10]), groundwater levels (e.g. Zhang et al. [13]),

and flood prediction (e.g. Le et al. [14]). These machine learning models are able to learn the relationship between meteorological forcing data (i.e. temperature, precipitation, evapotranspiration, etc.) and surface water runoff without requiring extensive in-situ static data (e.g. soil type, land cover, slope, etc.). Kratzert et al. [15] even demonstrate that physical basin characteristics (which would have otherwise been the inputs for a traditional hydrological model) can be inferred from the learned weights of the trained network.

We design and implement a bayesian sequence-to-sequence-to-sequence long short-term memory (LSTM)[16] deep neural network with a graph convolutional header to predict daily volumetric reservoir water availability changes in sixty-six reservoirs across ten river basin networks in India. Our machine learning approach has several novelties. Using multiple concatenated sequence architectures allows both historic and ex-ante forecast data to be used to condition hidden state variables while facilitating an arbitrary prediction horizon. The probabilistic conditioning allows model uncertainty to be communicated to the end user. The graph convolution header facilitates model conditioning that is aware of the hydrological adjacency of the basin network component basins. Lastly, our model is autocorrelative – current reservoir levels are an important input feature to the model.

We obtain near-real-time surface water availability measurements from the India Water Resources Information System (WRIS)[17], historic precipitation data from the Climate Hazards Center, UC Santa Barbara [18], and historic and ex-ante forecast meteorological forcing data from the European Centre for Medium-Range Weather Forecasts (ECMWF) [19, 20]. We train our model on seven years of historic data, and cross-validate and test on two years each. The resulting model performs well on held-back test data, with average coefficients of determination across all sites in excess of 33% for time horizons out to ninety days. We operationalise the trained model, ingesting data in near-real-time and distributing model inference via an API and user interface. The model and operationalised services won the Wave2Web hackathon in September 2021, facilitated by the World Resources Institute and sponsored by Microsoft and BlackRock.

2. Methods

Our Bayesian sequence-to-sequence-to-sequence LSTM is conceptually similar to the sequence-to-sequence model of Xiang et al. [21], which in turn

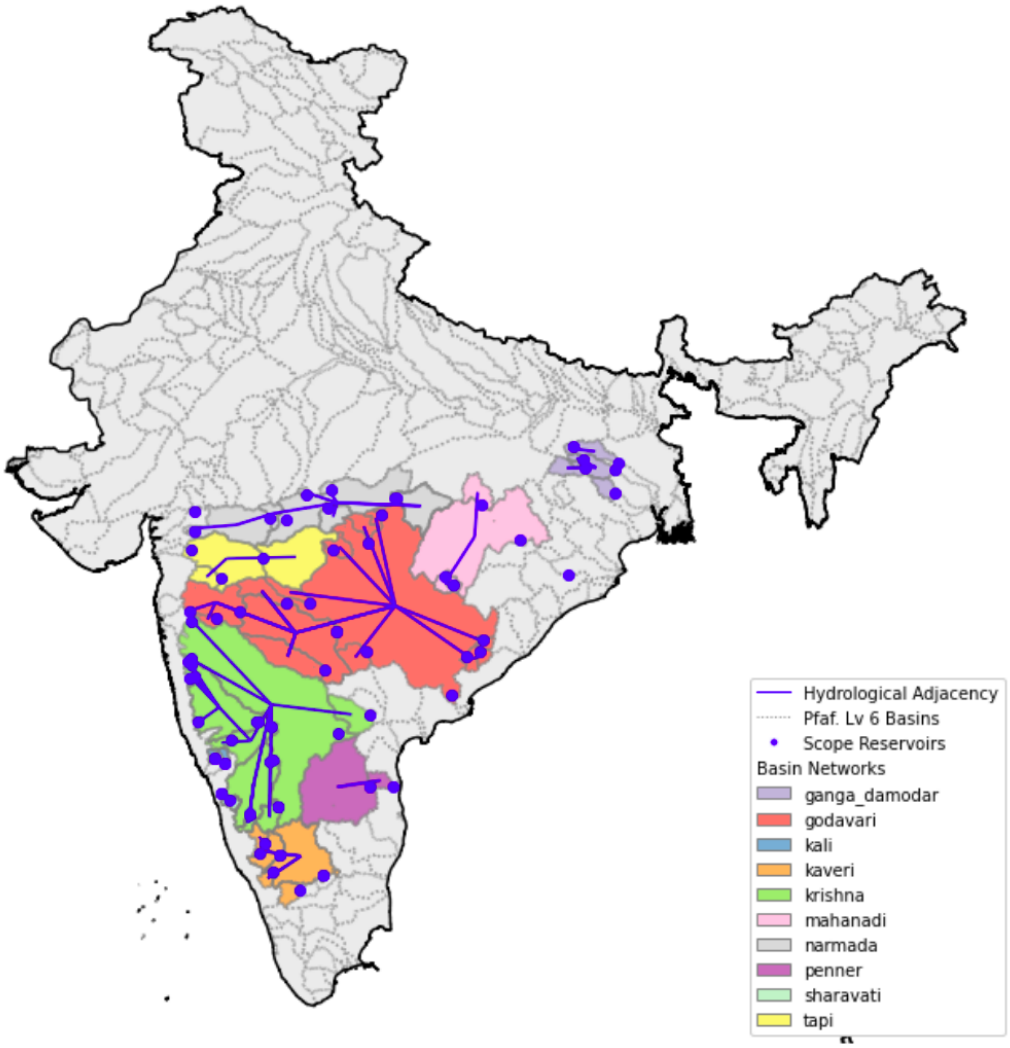

Figure 1: **India Study Area** showing ten basin networks, hydrological adjacency, scope reservoirs, and Pfafstetter Level 6 waterbasins.

is inspired by the original Seq2Seq model of Sutskever et al. [22]. Like Xiang et al. [21], our model features encoder and decoder stages with an intermediary encoded hidden state being passed between the two components. We add an additional sequence decoder beyond the forecast data horizon to allow predictions to an arbitrary horizon. The encoder stage is comprised of an LSTM that is conditioned on historical meteorological forcing data, specifically the daily mean temperature and precipitation of each reservoir's specific upstream area. By 'specific' upstream area we refer to the upstream area of each reservoir that is not also upstream of an upstream reservoir, see Appendix A for details. The model is autocorrelative; the historic reservoir levels, rescaled to [0,1] are concatenated to the historic meteorological forcing data. The first decoder stage is the 'forecast' LSTM decoder. The 'forecast' decoder inherits hidden state representations from the encoder and is conditioned on forecast mean temperature and precipitation which are geospatially reduced in the same manner as the historic data. Both historic and forecast precipitation is z-scored by dividing by the reservoir-wise standard deviation; temperature data is z-scored by subtracting the reservoir-wise mean and then similarly dividing by the reservoir-wise standard deviation.

The final stage is the 'future' LSTM decoder. This final stage is necessary because the forecast data is only available fourteen days into the future, and the desired prediction horizon is ninety days. The 'future' decoder inherits hidden state representations from the 'forecast' decoder and has no meteorological conditioning data. In this way all the predictive information about the future reservoir state must be encoded into the hidden state representations passed between encoder and decoder stages.

The outputs of the 'forecast' and 'future' LSTM decoders are passed through a graph convolutional output header composed of two linear layers with bias and dropout, and an intermediary graph conovolutional layer. The linear headers are applied reservoir-wise such that each reservoir has its own linear header. The graph convolutional layer traverses information between the reservoirs using the directional basin adjacency graph obtained from the HydroSHEDS basin network data[23]. The adjacency matrix is populated with positive unity values for downstream edges, negative values for upstream edges, and positive values along the diagonal. The same header is used for both the 'forecast' and 'future' decoders, forcing semantic congruence between the decoder outputs. The targets of the machine learning model are the daily reservoir availability changes, representative of the net inflow and outflow in billion cubic meters, z-scored by subtracting the mean difference

and dividing by standard deviation (on the already [0,1] normalised water volumes). All model stages are also conditioned with climatological data; the sine and cosine of the periodic day-of-the-year are concatenated to the input data (and are the only input data for the 'future' decoder). In forward operations, the daily predicted reservoir availability change is de-z-scored and added to the previous day's reservoir level. The previous day's reservoir level is concatenated as an input feature to the output header to give the conditioning awareness of current reservoir levels.

Multiple models are trained, one for each basin network (i.e. one for each connected component of the hydrological graph). The entire model is probabilistic: each weight in the LSTM is normally distributed with a mean and standard deviation. The loss function is thus comprised of two components: mean-squared error as the maximum-likelihood component, and KL divergence as the complexity loss, as developed by Blundell et al. [24]. In training, the optimizer step minimises both loss terms. Complexity loss is normalised by the batch size and an additional weighting hyperparameter. After experimentation, we choose a weight to give a strong bias to maximum likelihood, ensuring convergence. At inference, a distribution can be obtained by repeatedly sampling the model, allowing model uncertainty to be communicated to the user. See supplemental material for more details on model architecture and training hyperparameters.

Reservoir water availability changes are predicted by conditioning the model on historic meteorological data and ex-ante forecast data. Both historic and forecast data are obtained from the European Centre for Medium-Range Weather Forecasts (ECMWF). Historic 2-meter surface air temperature and total precipitation data is obtained from the ERA5Land catalog. ERA5Land is a spatial upsampling of the ERA5 reanalysis catalog which is provided at hourly resolution for the Earth's land surface area. The spatial resolution of ERA5Land is approximately 9km. Forecast data, likewise 2-meter surface air temperature and total precipitation, is obtained from the TIGGE global ensemble[20]. The TIGGE ensemble is available at 0.5^o spatial resolution up to 14 days in the future in six-hour time steps. Daily historic precipitation data is also obtained from the CHIRPS dataset[18], with a spatial resolution of 0.05^o. In the final data service, CHIRPS precipitation and TIGGE initial two-meter temperature is used for historic forcing due to ERA5Land being unavailable in near-real-time. Reservoir water availability data is obtained from India-WRIS, a project funded by the India Central Water Commission.

The conditioning period is from 2010 through the end of 2021. The years of 2013 and 2018 are used as cross-validation years; 2011 and 2020 are reserved as test years; the remainder of the years are used for training. Entire years are used for cross-validation and test to capture the periodicity of the conditioning data. Corrupt data records in the TIGGE archive prevent most of 2017 from being useable. After masking missing data and trimming for the historic and prediction horizons, the resulting dataframes are 4204 days long, with 730 each held back for validation and testing, although missing data results in slightly less data for some sites.

Data are ingested in as-close-to real time as possible to facilitate prediction of water levels for anticipatory action. The ECMWF data is updated daily with a two-day lag. The India WRIS levels are updated irregularly, approximately every five to ten days. CHIRPS data are updated every five days with a one-day lag. This means in practise the predictions available from the published service have at least a six-day lag. Increasing the update frequency and decreasing the lag would help improve prediction accuracy for decision-making.

3. Findings

In general, we find a large variability in the ability of our model to predict reservoir water availability changes up to ninety days in the future. Best-performing basin networks were narmada, sharavati, and godavari; basin networks in the north of India with a high number of interconnected reservoirs and moderate amounts of rain. The best performing reservoirs among the total full population of sixty-six were bhatghar, dudhganga, linganamakki, kolar, and mula. The worst-performing basin networks were ganga damodar and penner, with tenughat, gerusoppa, vanivilasa sagar, khadakwasla, and mettur as the worst-performing individual reservoirs. See Table 1 for a comparison of predictive performance by basin network.

Better performing reservoirs and basin networks were those where changes in the reservoir water availability were smooth and continuous, and were clearly seasonal and driven by meteorological phenomena. In the worst performing reservoirs and basin networks, the operation of the reservoir causes reservoir water availability changes which are uncorrelated with meteorological or even periodic signals in the input data. The cases where reservoir water availability is uncorrelated with meteorological data should be inspected further as an edge case. See Figure B.8 for example timeseries of predictions,

and Figure A.4 for example input and target data.

The model had a difficult job; the machine learning task was to learn *net* reservoir water availability changes. Inflows might be expected to directly related to upstream meteorological forcing, but outflows are also dependent on downstream water demand and manual reservoir operation. In general, we see that the model learns more accurate short-term predictions of reservoir water availability changes. In the medium- and long-term (20 to 90 days) model performance deteriorates. Table 1 compares performance of each basin network at different prediction horizons. At the longer time horizons, model performance improves slightly as climateological mean-reversion begins to dominate over short-term encoded hydrological states. Future work should explore the machine learning model further and make results more explainable - leading to a better understanding of model performance, uncertainty, and where better data could lead to more accurate model predictions.

We perform an ablation study to investigate the contribution of the graph convolutional layer to overall model accuracy. To test this, we retrain the models for each basin network without the graph convolutional layer, allowing the first linear layer to feed forward directly into the second. We compare predictions between the trained models with the lowest validation loss checkpoints for each model configuration and basin network. We find that the ablation of the graph convolutional layer *increases* model performance by 0.82 percentage points, averaged across all reservoirs and prediction horizons. Figure 3 shows model performance for baseline and graph convolution-ablated models for all reservoirs against prediction horizon. The deterioration in performance observed in the graph convolution ablation test suggests that the model is perhaps overfit overall, and the mechanism of graph convolution does not immediately and naturally traverse information about how 'full' upstream reservoirs are to the prediction of downstream changes in reservoir water availability.

We assess the uncertainty estimation of our models using monte carlo simulation. We show, for example in Figure B.8 the $\mp 95\%$ confidence interval of the sampled paths. Figure 2 shows the uncertainty correction and 95% confidence interval as a function of prediction horizon, and the observed volumetric reservoir water availability change. Panel (a) shows that the largest model uncertainty is predicted for the nearest-term timesteps. Because of our heavy bias towards maximum likelihood (rather than uncertainty) estimation, we define a correction factor at each site and prediction horizon, which is required to stretch the uncertainty bounds to include the observed

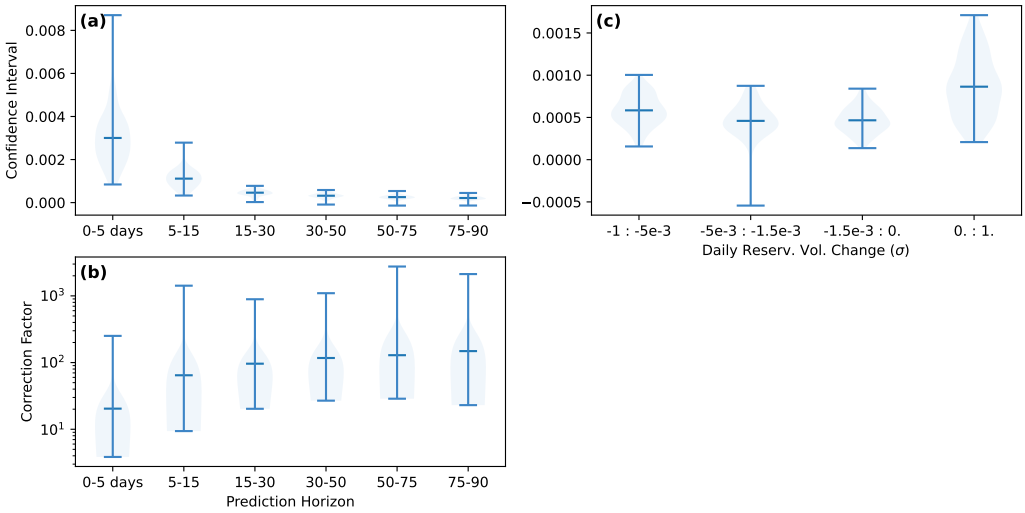

Figure 2: **Uncertainty Metrics:** uncertainty correction and confidence interval as a function of prediction horizon and the observed reservoir water availability change.

timeseries (Panel (b)). The correction factor is greatest for all sites at the most distant prediction horizons. The combination of panels (a) and (b) suggest that model uncertainty is not being propagated deep into the model. Panel (c) shows the relationship of moel uncertainty to the observed reservoir water availability change. When the volumetric change is large and positive, i.e. when the reservoir is filling, the model uncertainty is the greatest.

4. Conclusion

Ninety-day predictive models are prepared for daily water availability changes in sixty-six reservoirs across ten basin networks in India. A data service is published which ingests data and offers publicly-available predictions in near-real-time. The accompanying codebases and dataframes are publicly released. To our knowledge, ours is the first publicly-available codebase to explicitly model hydrological adjacency via graph convolutions. Our data service has been made publicly available to facilitate better water security decision-making. Data services such as ours can help improve adaptation and resilience to the water security impacts of our changing climate.

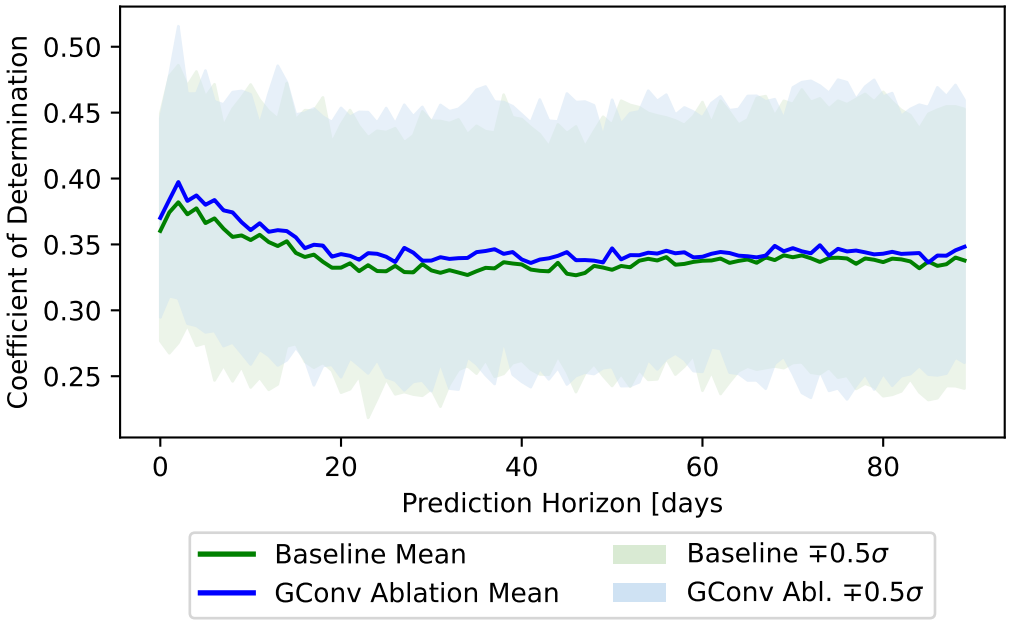

Figure 3: **Test-set prediction coefficient of determination** for baseline and graph convolution ablated models, predicted vs. realised normalised changes in reservoir water availability. The reservoir-wise mean and half standard deviation are shown.

Table 1: **Test-Set Coefficient of Determination** for ten basin networks, selected prediction horizons

Basin Network	Prediction Horizon, days **1-5**	**5-20**	**20-50**	**50-90**	Reservoirs (N)
Ganga Damodar	0.21	0.18	0.19	0.21	periyar, maithon, tenughat$^-$, kangsabati, konar$^+$, tilaiya (6)
Godavari	0.39	0.37	0.36	0.36	sriramsagar, jayakwadi nath sagar, yeldari, lower manair g v sudhakar rao, balimela$^-$, pench, isapur, upper wardha, mula$^+$, sanjay sarovar upper wainganga, machkund jalaput, upper kolab, bhandardara (13)
Kali	0.40	0.36	0.31	0.30	yeleru, upper indrawati$^+$, supa$^-$ (3)
Kaveri	0.41	0.37	0.33	0.33	narayanapura, mettur$^-$, krishnaraja sagar, lower bhawani, hemavathy$^+$, kabini, harangi (7)
Krishna	0.36	0.38	0.35	0.35	nagarjuna sagar, srisailam, panchet, almatti, khadakwasla, tungabhadra, ghatprabha hidkal, vanivilasa sagar$^-$, malaprabha, bhadra, bhima ujjani, koyana shivaji sagar, bhatghar, dhom, dudhganga$^+$, manikdoh, urmodi, niradevghar (18)
Mahanadi	0.40	0.35	0.34	0.34	hirakud, minimata bangoi hasdeo$^-$, mahanadi ravishankar sagar$^+$ (3)
Narmada	0.39	0.36	0.36	0.42	karjan, sardar sarovar$^-$, indirasagar, bargi, tawa, barna, kolar$^+$, sukhi tank (8)
Penner	0.32	0.29	0.31	0.29	somasila (1)
Sharavati	0.49	0.39	0.36	0.35	gerusoppa$^-$, linganamakki$^+$, sholayar (3)
Tapi	0.39	0.38	0.30	0.29	ukai$^-$, upper tapi hatnur, girna$^+$ (3)

$^+$: best of basin network; $^-$: worst of basin network

5. Data Availability

All data used in this work is obtained from publicly available sources. The dataframes used to train each basin network are publicly available at gs://oxeo-public/wave2web/h2ox-ai. The trained models are available via github at https://github.com/H2Oxford/h2ox-ai/tree/main/models. Model inference is provided in near-real-time via the api.h2ox.org data service. Documentation for this service can be found at api.h2ox.org/docs. Access to intermediary BigQuery tables and Cloud Storage Zarr archives can be made available on request.

6. Code Availability

All code used for the preparation of this paper and the h2ox.org data service is publicly available at https://github.com/H2Oxford/. This github organization includes eight repositories which together comprise the H2Ox data service: h2ox-data, h2ox-forecast, h2ox-chrips, h2ox-reducer, h2ox-w2w, h2ox-ai, h2ox-api, and h2ox-dash. The contents of each repository are summarised in the organisation README page, and each repository also has a README with documentation and steps for reproduction.

7. Author Contributions

Dr Lucas Kruitwagen was the team leader of H2Ox, designed and built the machine learning model, designed and built the data service, and wrote the paper draft. Chris Arderne designed the machine learning model, designed and built the data service, and edited the paper draft. Dr Thomas Lees designed and built the machine learning model, designed the data service, and wrote the paper draft. Dr Elizabeth Thalheimer designed the machine learning model, designed the data service, and edited the paper draft. Samantha Kuzma designed the data service and edited the paper draft. Samrat Basak edited the paper draft.

Appendix A. Data Description

ERA5 Land [19] is a global reanalysis product produced by the European Centre for Medium Range Weather Forecasting (ECMWF) for describing the water and energy cycles. A reanalysis product is produced by combining observations from multiple sources (in-situ, satellites etc.) with a global circulation model to provide a global, spatially consistent, gridded data product. ERA5 Land is produced by reprocessing the land surface components of the model forced by the ERA5 atmospheric reanalysis data to produce a product with 9km grid spacing and an hourly temporal frequency [19]. This improved spatial resolution is important for simulating hydrological behaviours in smaller catchments, and an improved representation of soil moisture and snow processes has led to the ERA5 Land dataset being used in various hydrological studies [25].

The TIGGE forecast [20] is a dataset consisting of ensemble forecasts from 10 global numerical weather prediction centers compiled for research purposes. The data is archived with ECMWF, and we use the ECMWF operational model provided with the data archive. The ECMWF model is a global ensemble system with 51 ensemble members perturbed with stochastic physics to represent uncertain process parameterisations in the model. It is run twice daily and produces forecasts up to 15 days into the future. 51 ensemble members are run at $50km^2$ grid resolution producing forecasts for 30minute intervals up to 15 days (0hrs, 0.5hrs, 1hrs, ..., 299.5hrs, 360hrs). This data is available 48hours after the initial time of the forecasts. TIGGE precipitation data is provided in cumulative measurements after the initial time, so the difference is first taken to obtain daily forecast precipitation values.

The India Water Resource Information System (India-WRIS)[17] provides near-real-time reservoir data with a lag of up to ten days. Water heights and volumes are provided for many of the major basins and catchment ares in india; a subset has been used in this study. Data is available via an API; each reservoir having a unique identifying number. The CHIRPS [18] precipitation dataset spans from 50^oS to 50^oN and combines satellite and ground station data to estimate daily precipitation with a spatial resolution of 0.05^o.

For the final models and data service, the TIGGE 2-meter temperature variable is used for both historic and forecast forcing. Six-hour forecast variables have been reduced to daily means. CHIRPS data is used for historic precipitation forcing, and TIGGE precipitation is used for forecast forcing.

Forecast and future time horizons are also forced with day-of-the-year periodicity, both sine and cosine components. Historic and future temperature data is z-scored by subtracting the reservoir-wise mean and dividing by the reservoir-wise standard deviation. Historic and future precipitation data is z-scored only be dividing by reservoir-wise standard deviation, given a one-side distribution. CHIRPS and TIGGE precipitation are z-scored separately. Reservoir water availabilities are normalised to the range of [0,1], and then the volumetric differences are z-scored by mean and standard deviation.

Only reservoirs where there is sufficient daily data are included in the model scope. Many reservoirs only had data from the last several years, not since 2010, so these reservoirs were excluded. Where data was missing, it was interpolated cubically between its closest neighbours. Up to 15 days of missing data was interpolated before the data was deemed invalid and removed from the scope time period. Dates that relied on the dates of the missing data, either in the historic encoding or future prediciton horizon were also removed.

ERA5, TIGGE, and CHIRPS data are all mirrored to cloud storage Zarr archives. These archives store very large volumes of compressed data in a way that makes for optimal distributed reading and writing. We rechunk these archives to be contiguous in the time domain, creating efficient distributed read-access for long timeseries over small geographies. This allows us to efficiently sample and reduce timeseries for upstream geometries. The archives are added-to continually in time by the respective data services.

Upstream areas for each reservoir were achieved by merging all Pfafstetter Level 8[23] basin geometries uniquely upstream of each reservoir. We merge all upstream basins of the farthest upstream reservoir first; then cascade down the hydrological graph merging the remaining upstream basin geometries for each reservoir which have not been already included in the upstream geometry of an upstream reservoir. The result is each basin flows into a single reservoir, and then the graph convolutions are trusted to traverse the flow along the hydrological graph. Geometric reduction was achieved by masking the Zarr archives with the rasterised upstream geometry of each reservoir. The weights of the rasterised mask were weighted with the portion of the intersection of the upstream geometry with the dataset grid cell (i.e. if the upstream geometry intersected only 40% of a given grid cell, that pixel of the mask was given a value of 40%). Mask weights were used for weighted reductions of the data to a single-dimension timeseries for each upstream area. Weighted sums were used for upstream precipitation; weighted means

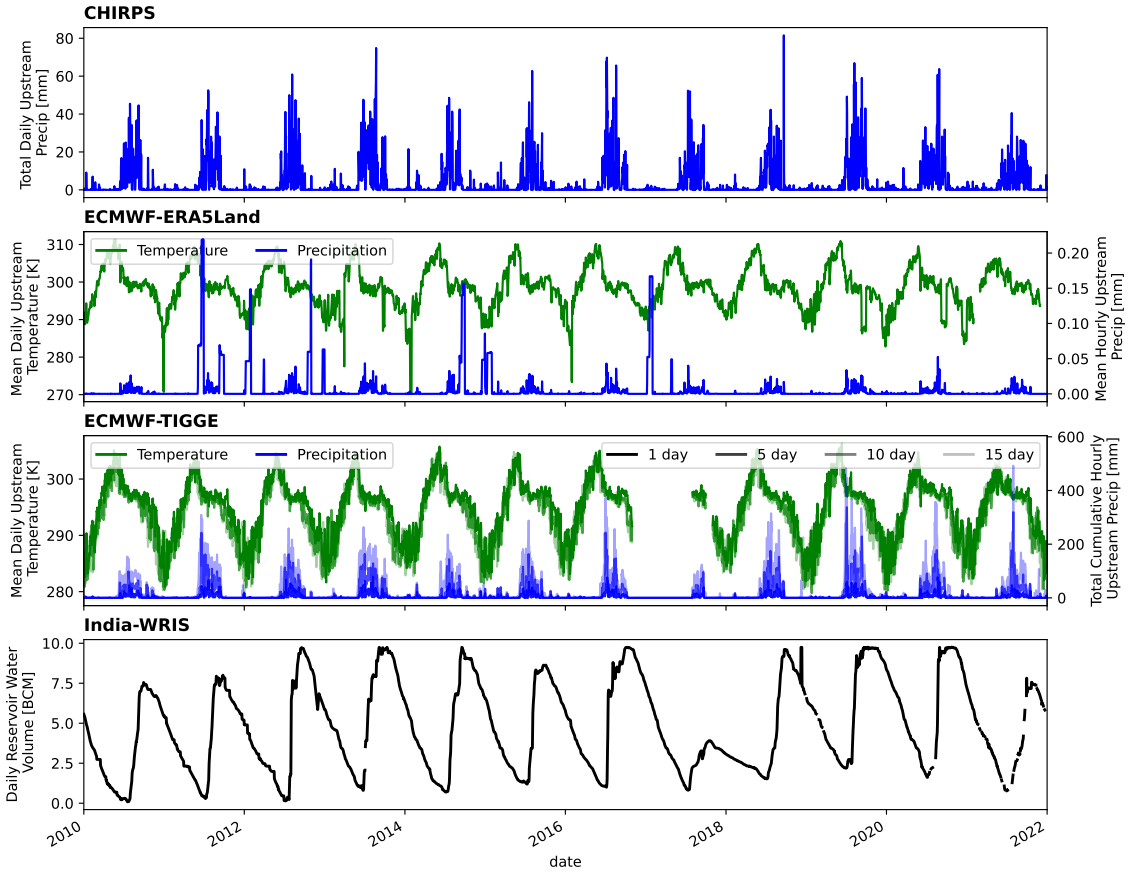

Figure A.4: **Sample data timeseries** showing reservoir water availability and upstream CHIRPS precipitation data, TIGGE forecast data, and reservoir water availabilties for Indira Sagar, the largest reservoir.

for temperature.

Appendix B. Model and Training Detailed Description

The bayesian LSTM sequence-to-sequence graph neural network combines the best-available neural network architectures for probabilistic prediction on objects with graph relationships. Many authors have used LSTMs for hydrological research (see Section 1). We use three LSTM sequences to encode historic and forecast data, while allowing for an arbitrary prediction horizon. We experimented with different LSTM designs: hidden state size, "peephole"

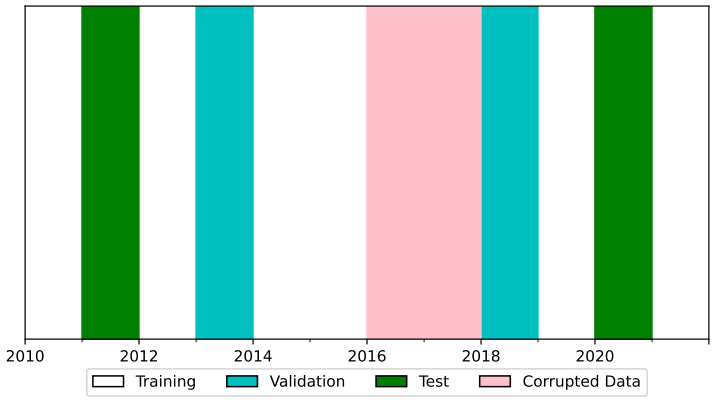

Figure A.5: **Train / Test / Validation Split** with the corrupted TIGGE data period in 2017.

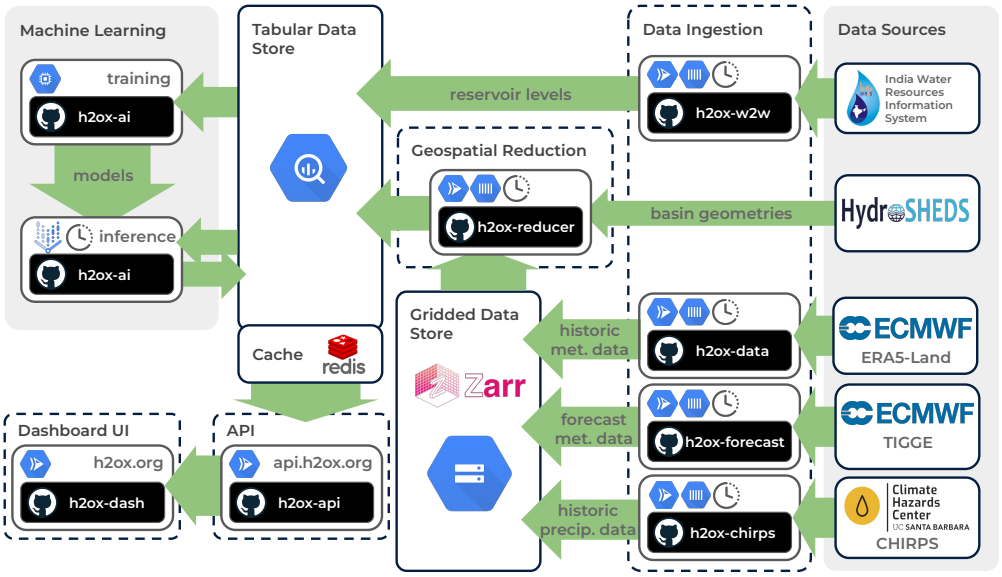

Figure A.6: **Data Service Architecture** showing the data sources, cloud services, and github repositories developed to serve near-real-time inference via (api.)h2ox.org.

connections[26], and number of layers. We found that a single-layer LSTM with a hidden state size several times larger than the input dimension, without peephole, gave the best cross-validation performance.

Adding probabilistic elements to our model allows us to estimate model uncertainty in our predictions. We use a Bayesian LSTM implementation from the Blitz Bayesian Deep Learning Python library [27]. Training the Bayesian neural network minimises the combined loss from maximum likelihood and complexity loss (proxied by Kullback-Liebler divergence)[24]. We experiment with the weighting of the complexity loss (relative to maximum likelihood loss), and the initial assumptions on the prior and posterior distributions. We find that by we need to significantly weight the loss function to likelihood loss, and relax the assumptions on prior and posterior distributions, to obtain reasonable convergence of the distribution expected values.

We include and test a graph convolutional header in our model implementation. The adjacency matrix for the graph convolutional header is constructed from the graph of basin adjacencies, where downstream basins have directed edges from all upstream basins. This reflects the logic that water must flow downstream from reservoir to reservoir, and reservoir inflows must be dependent on outflows of upstream basins. The adjacency graph also includes unity values on the diagonal to traverse inflow information across the graph convolution step, and also negative unity values across the diagonal (i.e. reversed directional edges) to traverse mass-flow information (whereby an outflow in one reservoir should be an inflow in a downstream reservoir). The graph convolutional header is preceeded and proceeded by a reservoir-wise linear layers with dropout and ReLU activations. Linear layers do not have bias weights. In experimentation it was found that bias weights enabled mean reversion which prevented convergence of the Bayesian layers.

The number of parameters for each model layer as a function of the number of reservoirs are shown in Table B.2. All model hyperparameters can be found in the configuration files in the codebase. The Krishna basin network, for example, with a hidden size of 12 and 18 reservoirs, has 52,200 parameters. The Kaveri basin, with 7 reservoirs, has 20,388 parameters.

In order to guard against overfitting and to fairly estimate the performance of the models, we split our data into three subsets, training data, validation data and test data (Fig. A.5). We use only the training data to update model weights, and the validation data is used to help find hyperparameters and check model fit. The test set is held out until after we have confirmed our model architecture and hyperparameters. We split our dataset

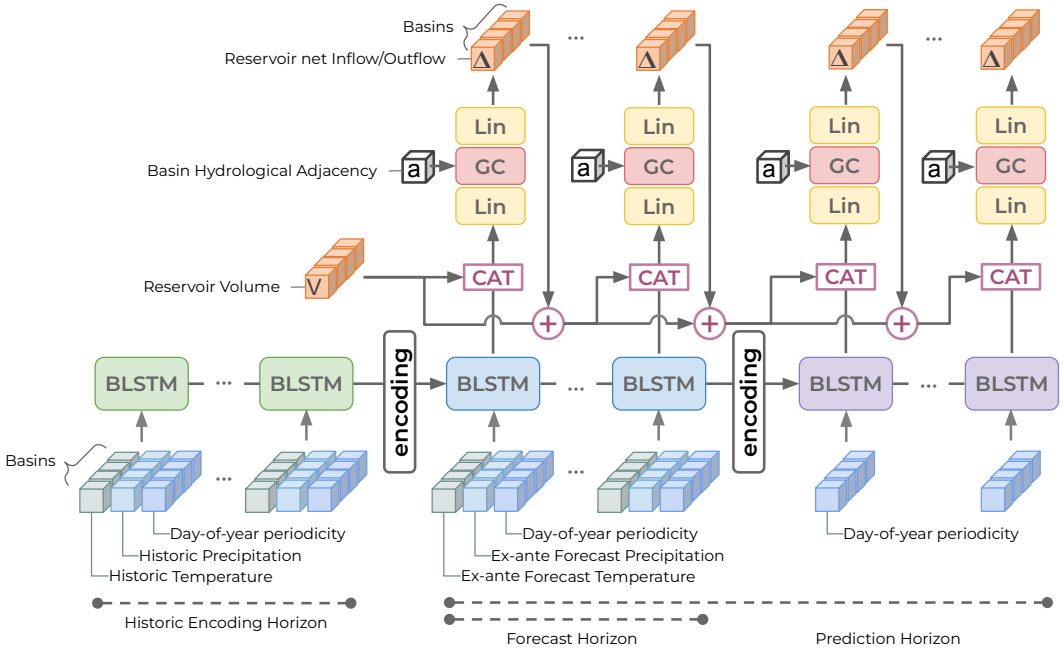

Figure B.7: **Machine learning model architecture** with three sequence stages, bayesian LSTM encodings, feed-forward differentials, and graph convolutions using basin hydrological adjacency.

by years, including 2010, 2012, 2014–2017, 2019, 2021 in our training data. We included 2013 and 2018 in our validation set. Our test set was made up of 2011 and 2020.

Model training proceeds for each basin network, with basin networks ranging from one to eighteen reservoirs. The model is implemented in PyTorch and trained on an NVidia V100 GPU. Training is monitored via Tensorboard and experiments are logged with Sacred. All training hyperparameters can be found in the configuration files in the codebase.

Appendix C. Graph Convolution Ablation Study

A key hypothesis of deep learning with hydrology is the use of graph relationships to better predict inflows and outflows (e.g. Kratzert et al. [28]). To test the impact of graph convolution on model results, we simply retrain each basin network model without graph convolution in the model header.

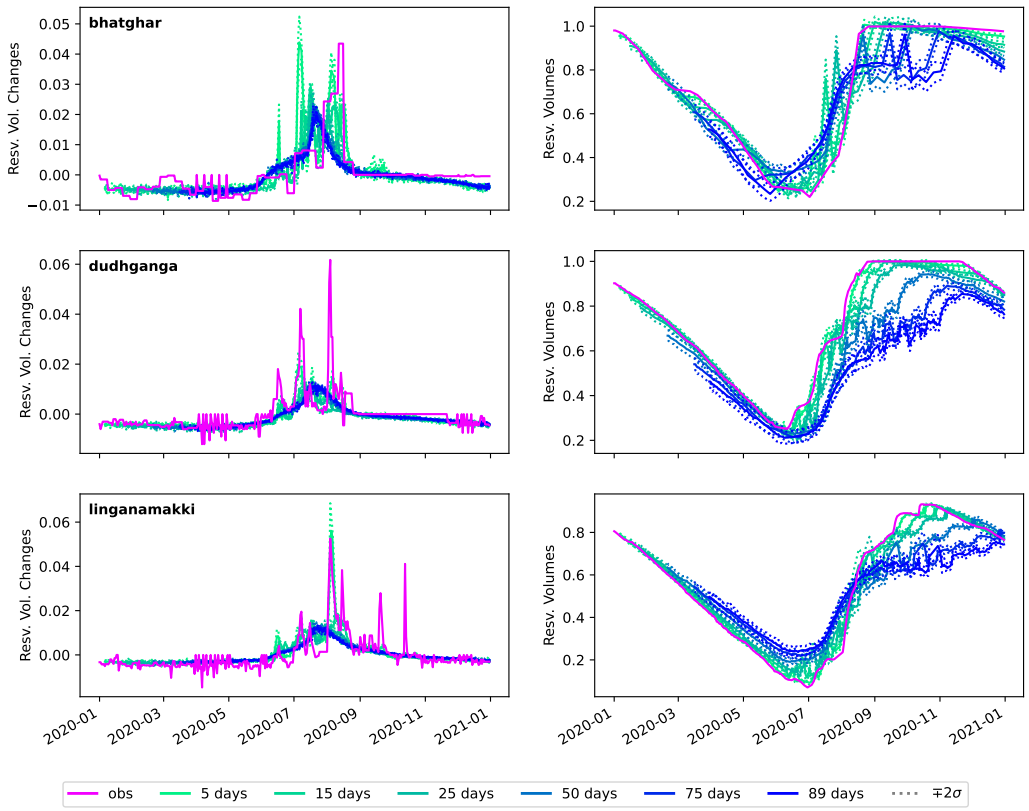

Figure B.8: **Test period predictions sample** showing predictions at incremental prediction horizons for top-three reservoirs (as ranked by mean coefficient of determination).

Table B.2: **Machine Learning Model Architecture**

Layer Name	Shape	Number of Parameters
INPUT		
-X_h	N x T_h x 4	-
-X_f	N x T_f x 4	-
-X_{ff}	N x T_{ff} x 4	-
ENCODER		
Bayesian LSTM	N x T_h x 12	-
-$U_{i,f,g,o\|\mu}$	-	4*4*HS*N
-$U_{i,f,g,o\|\rho}$	-	4*4*HS*N
-$W_{i,f,g,o\|\mu}$	-	4*4*HS*N
-$W_{i,f,g,o\|\rho}$	-	4*4*HS*N
-$\beta_{i,f,g,o\|\mu}$	-	4*HS*N
-$\beta_{i,f,g,o\|\rho}$	-	4*HS*N
DECODER x 2		
Bayesian LSTM	N x $T_{f,ff}$ x 12	-
-$U_{i,f,g,o\|\mu}$	-	4*4*HS*N
-$U_{i,f,g,o\|\rho}$	-	4*4*HS*N
-$W_{i,f,g,o\|\mu}$	-	4*4*HS*N
-$W_{i,f,g,o\|\rho}$	-	4*4*HS*N
-$\beta_{i,f,g,o\|\mu}$	-	4*HS*N
-$\beta_{i,f,g,o\|\rho}$	-	4*HS*N
HEADER		
$\text{Linear}_{no-bias}$	-	(HS+1)*HS*N
GNN	-	HS*HS
$\text{Linear}_{no-bias}$	-	HS*1*N
	TOTAL	HS*(2HS*N+HS+217N)

T_h: historic encoding horizon; T_f: forecast data horizon; T_{ff}: future horizon.

Because the graph convolution input and output size is the same shape, the graph convolutional layer can simply be removed to conduct an ablation study. In the figures in this draft, the model checkpoint with the lowest validation loss is used, including when comparing models in the ablation study.

References

[1] A. Boretti, L. Rosa, Reassessing the projections of the world water development report, NPJ Clean Water 2 (2019) 1–6.

[2] A. F. Van Loon, Hydrological drought explained, Wiley Interdisciplinary Reviews: Water 2 (2015) 359–392.

[3] R. W. Hofste, S. Kuzma, S. Walker, E. H. Sutanudjaja, M. F. Bierkens, M. J. Kuijper, M. F. Sanchez, R. Van Beek, Y. Wada, S. G. Rodriguez, et al., Aqueduct 3.0: Updated decision-relevant global water risk indicators, World Resources Institute: Washington, DC, USA (2019).

[4] M. Schiavina, S. Freire, K. MacManus, Ghs population grid multitemporal (1975, 1990, 2000, 2015), 2019. URL: `http://data.europa.eu/89h/0c6b9751-a71f-4062-830b-43c9f432370f`. doi:`10.2905/42E8BE89-54FF-464E-BE7B-BF9E64DA5218`.

[5] T. Birch, S. P. Brumby, C. F. Brown, C. Hanson, Dynamic world: Modern methods of applying neural networks to automate global land cover mapping, in: Google GeoforGood 2020, 2020.

[6] L. Byers, J. Friedrich, R. Hennig, A. Kressig, X. Li, C. McCormick, L. M. Valeri, A Global Database of Power Plants, Technical Report, Washington DC, USA, 2018. doi:`https://www.wri.org/publication/global-power-plant-database`.

[7] F. Callister, Beneath the surface: the state of the world's water 2019 (2019).

[8] T. Daniell, Neural networks. applications in hydrology and water resources engineering, in: National Conference Publication- Institute of Engineers. Australia, 1991.

[9] D. Nagesh Kumar, K. Srinivasa Raju, T. Sathish, River flow forecasting using recurrent neural networks, Water resources management 18 (2004) 143–161.

[10] F. Kratzert, D. Klotz, C. Brenner, K. Schulz, M. Herrnegger, Rainfall–runoff modelling using long short-term memory (lstm) networks, Hydrology and Earth System Sciences 22 (2018) 6005–6022.

[11] C. Shen, A transdisciplinary review of deep learning research and its relevance for water resources scientists, Water Resources Research 54 (2018) 8558–8593.

[12] H. Fan, M. Jiang, L. Xu, H. Zhu, J. Cheng, J. Jiang, Comparison of long short term memory networks and the hydrological model in runoff simulation, Water 12 (2020) 175.

[13] J. Zhang, Y. Zhu, X. Zhang, M. Ye, J. Yang, Developing a long short-term memory (lstm) based model for predicting water table depth in agricultural areas, Journal of hydrology 561 (2018) 918–929.

[14] X.-H. Le, H. V. Ho, G. Lee, S. Jung, Application of long short-term memory (lstm) neural network for flood forecasting, Water 11 (2019) 1387.

[15] F. Kratzert, D. Klotz, G. Shalev, G. Klambauer, S. Hochreiter, G. Nearing, Towards learning universal, regional, and local hydrological behaviors via machine learning applied to large-sample datasets, Hydrology and Earth System Sciences 23 (2019) 5089–5110.

[16] S. Hochreiter, J. Schmidhuber, Long short-term memory, Neural computation 9 (1997) 1735–1780.

[17] I. W. R. I. System, India-wris: Reservoir level, 2008. URL: `https://indiawris.gov.in/wris/#/Reservoirs`.

[18] C. Funk, P. Peterson, M. Landsfeld, D. Pedreros, J. Verdin, S. Shukla, G. Husak, J. Rowland, L. Harrison, A. Hoell, et al., The climate hazards infrared precipitation with stations—a new environmental record for monitoring extremes, Scientific data 2 (2015) 1–21.

[19] J. Muñoz-Sabater, E. Dutra, A. Agustí-Panareda, C. Albergel, G. Arduini, G. Balsamo, S. Boussetta, M. Choulga, S. Harrigan, H. Hersbach, et al., Era5-land: A state-of-the-art global reanalysis dataset for land applications, Earth System Science Data 13 (2021) 4349–4383.

[20] R. Swinbank, M. Kyouda, P. Buchanan, L. Froude, T. M. Hamill, T. D. Hewson, J. H. Keller, M. Matsueda, J. Methven, F. Pappenberger, et al., The tigge project and its achievements, Bulletin of the American Meteorological Society 97 (2016) 49–67.

[21] Z. Xiang, J. Yan, I. Demir, A rainfall-runoff model with lstm-based sequence-to-sequence learning, Water resources research 56 (2020) e2019WR025326.

[22] I. Sutskever, O. Vinyals, Q. V. Le, Sequence to sequence learning with neural networks, Advances in neural information processing systems 27 (2014).

[23] B. Lehner, K. Verdin, A. Jarvis, New global hydrography derived from spaceborne elevation data, Eos, Transactions American Geophysical Union 89 (2008) 93–94.

[24] C. Blundell, J. Cornebise, K. Kavukcuoglu, D. Wierstra, Weight uncertainty in neural network, in: International conference on machine learning, PMLR, 2015, pp. 1613–1622.

[25] T. Lees, S. Reece, F. Kratzert, D. Klotz, M. Gauch, J. De Bruijn, R. Kumar Sahu, P. Greve, L. Slater, S. Dadson, Hydrological concept formation inside long short-term memory (lstm) networks, Hydrology and Earth System Sciences Discussions (2021) 1–37.

[26] F. A. Gers, J. Schmidhuber, F. Cummins, Learning to forget: Continual prediction with lstm, Neural computation 12 (2000) 2451–2471.

[27] P. Esposito, Blitz - bayesian layers in torch zoo (a bayesian deep learing library for torch), `https://github.com/piEsposito/blitz-bayesian-deep-learning/`, 2020.

[28] F. Kratzert, D. Klotz, M. Gauch, C. Klingler, G. Nearing, S. Hochreiter, Large-scale river network modeling using graph neural networks, in: EGU General Assembly 2021, 2021. doi:`10.5194/egusphere-egu21-13375`.